

RESEARCH

Open Access



miR-155 mediated regulation of PKG1 and its implications on cell invasion, migration, and apoptosis in preeclampsia through NF- κ B pathway

Xiaohua Luo^{1*}, Xiaopei Guo¹, Ningning Chen¹, Rui Peng², Ci Pan¹, Zhuyin Li¹, Bing Zhao¹, Ruonan Ji¹ and Siyu Li¹

Abstract

Background Preeclampsia (PE) is a severe pregnancy complication characterized by complex molecular interactions. Understanding these interactions is crucial for developing effective therapeutic strategies.

Methods This study applies a pharmacometabolomics approach to explore the roles of miR-155 and PKG1 in PE, focusing on the regulatory influence of the NF- κ B signaling pathway. Blood metabolomic profiles were analyzed, and bioinformatics tools, IHC staining, Western blot (WB) analysis, and immunofluorescence (IF) localization were employed to determine the expression and function of miR-155 and PKG1. Cell invasion, migration, proliferation, and apoptosis assays were conducted to assess miR-155's modulation of PKG1. Additionally, RT-qPCR and WB analysis elucidated NF- κ B-mediated regulation mechanisms.

Results Our findings indicate significant metabolic alterations associated with miR-155 modulation of PKG1, with NF- κ B acting as a critical upstream regulator. The study demonstrates that miR-155 affects cellular functions such as invasion, migration, proliferation, and apoptosis through PKG1 modulation. Furthermore, the NF- κ B signaling pathway regulates miR-155 expression, contributing to the pathological processes of PE.

Conclusion This study provides a proof of concept for using pharmacometabolomics to understand the molecular mechanisms of PE, suggesting new therapeutic targets and advancing personalized medicine approaches. These insights highlight the potential of pharmacometabolomics to complement genomic and transcriptional data in disease characterization and treatment strategies, offering new avenues for therapeutic intervention in PE.

Keywords Preeclampsia, NF- κ B signaling pathway, miR-155 regulation, PKG1 expression, Cell behavior modulation

Introduction

Pre-eclampsia (PE) is a severe pregnancy complication characterized by hypertension, proteinuria, and systemic inflammation, posing serious risks to the health of both the pregnant woman and the fetus [1, 2]. Research suggests that the occurrence of PE may be closely linked to abnormal gene expression and disruption of cellular signaling pathways. Additionally, PE pregnancies are often associated with increased

*Correspondence:

Xiaohua Luo
luoxiaohua620@zzu.edu.cn

¹ Department of Obstetrics and Gynaecology, The Third Affiliated Hospital of Zhengzhou University, No.7 Kangfuqian Street, Erqi District, Zhengzhou 450052, Henan, China

² Scientific Research Department, The Third Affiliated Hospital of Zhengzhou University, Zhengzhou 450052, Henan, China



© The Author(s) 2024. **Open Access** This article is licensed under a Creative Commons Attribution-NonCommercial-NoDerivatives 4.0 International License, which permits any non-commercial use, sharing, distribution and reproduction in any medium or format, as long as you give appropriate credit to the original author(s) and the source, provide a link to the Creative Commons licence, and indicate if you modified the licensed material. You do not have permission under this licence to share adapted material derived from this article or parts of it. The images or other third party material in this article are included in the article's Creative Commons licence, unless indicated otherwise in a credit line to the material. If material is not included in the article's Creative Commons licence and your intended use is not permitted by statutory regulation or exceeds the permitted use, you will need to obtain permission directly from the copyright holder. To view a copy of this licence, visit <http://creativecommons.org/licenses/by-nc-nd/4.0/>.

oxidative stress [3] and placental hypoxia [4]. Risk factors for PE include a history of previous PE pregnancies, high body mass index (BMI), advanced maternal age, and paternal factors [5, 6], collectively underscore the complex pathophysiological mechanisms of pre-eclampsia.

Moreover, studies have indicated a close association between the occurrence of preeclampsia (PE) and abnormalities in gene expression and disruptions in cellular signaling pathways [7–9]. microRNAs (miRNAs), a crucial class of non-coding RNAs, play key regulatory roles in cellular biology and the development of diseases [10]. Among these, miR-155, a well-studied miRNA, has been shown to play significant roles in various diseases, yet its specific mechanisms in the pathogenesis of PE remain incompletely understood [11–13]. Through modulation of the expression of multiple target genes, miR-155 is believed to be involved in regulating essential biological processes such as cell proliferation, apoptosis, and inflammatory responses, playing a critical role in the pathophysiology of PE [14, 15]. A comprehensive investigation into the regulatory mechanisms of miR-155 in the development of PE can enhance our understanding of the pathological processes of PE and provide a vital theoretical foundation for the future development of therapeutic strategies targeting PE [11–13].

PKG1, also known as PKG1, plays a crucial role as a cellular signaling molecule in regulating various biological processes such as apoptosis, proliferation, and vascular smooth muscle relaxation [16]. In the context of PE, the expression level and activity of PKG1 may be regulated by miRNAs. Specifically, miR-155, as a potential regulatory factor, may play a critical role in the pathogenesis of PE through its regulation of PKG1 [17]. The regulatory effect of miR-155 on PKG1 could lead to abnormal expression or changes in activity, thereby affecting the normal functioning of the intracellular cGMP signaling pathway [17]. This aberrant signal transduction often results in intracellular imbalance, leading to a series of abnormal physiological responses, including increased apoptosis, limited proliferation, and enhanced vascular tension, which could potentially contribute to the onset and progression of PE [18, 19]. Therefore, investigating the regulatory mechanism of miR-155 on PKG1 and their interaction in the pathological process of PE is of significant importance for a deeper understanding of the pathogenesis of PE and for the research and development of therapeutic approaches related to PE [17].

NF- κ B, a critical transcription factor, plays an important role in regulating key physiological processes such as inflammation, immune response, and apoptosis [20–22]. In PE, the activation level of NF- κ B is closely associated with the onset and progression of this disease [23, 24].

This study aims to explore the regulatory role of miR-155 on PKG1 in the pathogenesis of PE and further investigate the role of NF- κ B in regulating miR-155 expression and influencing PKG1 levels. Through multidimensional analysis from the molecular level to cellular behavior, we expect to unveil the complex interactions among miR-155, PKG1, and NF- κ B. This research not only promises to provide new insights into the pathogenesis of PE but also offers a scientific basis for developing new therapies for the disease. By thoroughly understanding the regulatory mechanism of miR-155 on PKG1 and the regulatory role of NF- κ B therein, we can provide more effective targeted treatments and interventions for the clinical management of PE. This study holds significant clinical and scientific importance and is poised to bring about breakthroughs in the treatment and management of PE.

Materials and methods

Establishment of the PE mouse model

For the construction of the PE mouse model, we utilized C57BL/6J mice aged 6 to 8 weeks (strain hnslkjd005, from Hunan Sleek Jinda Experimental Animal Limited Company, Changsha). These mice were housed under pathogen-free conditions, with ad libitum access to food and water, following a 12-h light–dark cycle. Female and male mice were co-housed at a 2:1 ratio overnight. The first day of pregnancy was determined by observing mating plugs, designated as E0.5. Post-mating, six pregnant mice were randomly selected from each group for the study, while the remaining were excluded. The animal experiments in this study strictly adhered to international and national ethical guidelines and regulations concerning animal research, ensuring respect and protection for the animals. The use of experimental animals was approved by the ethics committee (Approval No: 2023-231-01), and all procedures were conducted according to laboratory animal experimental protocols to minimize animal distress and suffering.

To induce the PE model, pregnant mice were subcutaneously injected with L-NAME (125 mg/kg, NG-nitro-L-arginine methyl ester hydrochloride, 51298-62-5, provided by MedChemExpress) starting from E10, and this process continued for 6 days. Following gastric lavage with PBS, the experimental mice were divided into two groups: the PLN group received L-NAME, while the CTRL group received the control treatment of PBS. The Am-treated mice also underwent L-NAME injections (AmLN group). Another set of mice was administered external AmEV (20 μ g per mouse) or an equivalent volume of PBS every alternate day until D16. After 2 weeks of treatment, female mice were co-housed with males as described. Pregnant mice that received PBS gastric lavage were randomly assigned to two groups: the PLN

group received L-NAME (n=6), and the Control group received an equivalent volume of PBS (n=6). The AmEV-treated mice were exposed to L-NAME from E10 to E16 (PE group, n=6). On D16, pregnant mice were anesthetized with sodium pentobarbital (1.5% w/v, 60 mg/kg body weight). Blood samples were collected and centrifuged at 3000×g and 4 °C for 15 min to obtain serum, followed by the dissection and weighing of fetuses, kidneys, and uteri.

The pregnant mice were divided into six groups, each comprising six individuals, as follows: the Control group (received saline injections of equivalent volume on days 5, 8, 10, 12, and 14), the PE group, the sh-NC group (administered LPS injections on days 5 and 10, with placental injections of 20 μL containing 4 nmol sh-NC from days 12 to 16), the sh-PKG1 group (administered LPS injections on days 5 and 10, with placental injections of 20 μL containing 4 nmol sh-PKG1 from days 12 to 16), the miR-155 antagomir+sh-NC group (administered LPS injections on days 5 and 10, with placental injections of 20 μL containing 2 nmol miR-155 antagomir and 4 nmol sh-NC), and the miR-155 antagomir+sh-PKG1 group (administered LPS injections on days 5 and 10, with placental injections of 20 μL containing 2 nmol miR-155 antagomir and 4 nmol sh-PKG1, detailed in Table S1). All animal experiments were independently replicated three times [25, 26].

Measurements were taken to assess blood pressure and urine protein levels in mice

To evaluate the specific symptoms of gestational hypertension, mice underwent examinations for blood pressure (BP) and urine protein levels. Indirect blood pressure in mice was measured using the tail-cuff plethysmography method with the Visitech System BP2000 (BP-2000, Beijing Mingxintong Biotechnology Co., Ltd.). Prior to the formal blood pressure measurements, all mice underwent a habituation period of at least 3 days on GD 5, 14, and 16, during which at least 5 consecutive blood pressure readings were taken. Simultaneously, at the same time points, quantitative analysis of urine protein concentration was conducted on 24-h urine samples from mice housed in metabolic cages using the Coomassie Brilliant Blue protein assay kit (SNM297, Beijing Baio Caibo Technology) following the manufacturer's instructions [27].

Evaluation of kidney and placenta morphology in mice

The kidneys of mice were fixed, embedded in paraffin, and sectioned into 3 μm thick slices. Hematoxylin and eosin (H&E) or periodic acid-Schiff (PAS) staining was performed to examine the morphology of the renal glomeruli. Placental tissues of mice were stained with H&E

or Masson's trichrome to assess placental morphology. Masson's trichrome staining was employed to visualize collagen deposition, appearing blue, while muscle and cytoplasm exhibited shades of red to pink [28, 29].

ELISA detection

In this study, enzyme-linked immunosorbent assay (ELISA) was employed to detect the levels of placental growth factor (PlGF), soluble fms-like tyrosine kinase-1 (sFlt-1), and tumor necrosis factor-alpha (TNF-α) in mouse plasma. The following kits were utilized: PlGF kit (KBR-hlk7524, Shanghai Keboray Biotechnology Co., Ltd.); sFlt-1 kit (QY-XS4075-1, Hangzhou Qiyu Biotechnology Co., Ltd.); TNF-α kit (YSY70220, Tianjin Yisenyan Biotechnology Co., Ltd.). According to the manufacturers' instructions, protein levels of PlGF, sFlt-1, and TNF-α were determined in mouse plasma [30].

High-throughput transcriptome sequencing and data analysis

Placental tissues from three Control mice and three PE mice underwent high-throughput transcriptome sequencing. The specific procedures were as follows: Total RNA was extracted from each sample using Trizol reagent (Catalog No: T9424, Sigma-Aldrich, USA) following the manufacturer's instructions. RNA concentration, purity, and integrity were measured using the Qubit®2.0 Fluorometer® (Life Technologies, CA, USA) with the Qubit® RNA analysis kit, Nanophotometer (IMPLEN, California, USA), and the RNA Nano 6000 analysis kit on the Bioanalyzer 2100 system (Agilent Technologies, Santa Clara, CA, USA) to ensure an A260/280 ratio between 1.8 and 2.0. Each sample had a total RNA content of 3 μg, serving as the input material for RNA sample preparation. Following the manufacturer's recommendations, cDNA libraries were prepared using the NEBNext®Ultra™ RNA Directional Library Prep Kit (E7760S, Gene Company, China) designed for Illumina, with the quality assessed on the Agilent Bioanalyzer 2100 system. Subsequently, sample clustering was performed using the TruSeq PE Cluster Kit v3 cBot HS (Illumina) on the cBot cluster generation system per the manufacturer's instructions. Upon completion of library preparation, sequencing was conducted on the Illumina-HiSeq 550 platform, generating 125 bp/150 bp paired-end reads [31].

Quality control and differential analysis of sequencing data

The quality of paired-end reads in the raw sequencing data was assessed using FastQC software version 0.11.8. Preprocessing of the raw data was performed with Cutadapt software version 1.18, involving the removal of Illumina sequencing adapters and poly(A) tail sequences.

Additionally, a perl script was utilized to eliminate reads with N content exceeding 5%. High-quality reads, defined as those with a base quality above 20 and accounting for 70% of the bases, were extracted using FASTX Toolkit software version 0.0.13. BMap software was employed to repair paired-end sequences. Subsequently, the filtered high-quality read fragments were aligned to the mouse reference genome using hisat2 software version 0.7.12.

For the analysis of differentially expressed genes (DEGs) based on high-throughput transcriptome sequencing data, the R package limma was utilized. Differential expression was determined using the criteria $\text{P}_{\text{adj}} < 0.05$ and $|\log_{2}\text{FC}| > 2$ [32].

RT-qPCR

Total RNA from various intestinal tissues was extracted using TRIzol (15,596,026, ThermoFisher, USA). The concentration and purity of the extracted RNA were assessed using a NanoDrop 2000 spectrophotometer (ND-2000, ThermoFisher, USA). The mRNA was reverse transcribed into cDNA following the protocol of the PrimeScript RT reagent Kit (RR047A, Takara, Japan). The synthesized cDNA was subjected to RT-qPCR analysis using the Fast SYBR Green PCR kit (11,736,059, ThermoFisher, USA) with three replicates per well. GAPDH was utilized as the internal reference gene for mRNA, while U6 was used for miRNA. The experimental group's gene expression relative to the control group was calculated using the $2^{-\Delta\Delta\text{Ct}}$ method, where $\Delta\Delta\text{Ct} = \Delta\text{Ct}(\text{experimental group}) - \Delta\text{Ct}(\text{control group})$, and $\Delta\text{Ct} = \text{Ct}(\text{target gene}) - \text{Ct}(\text{reference gene})$. Ct represents the cycle threshold when the real-time fluorescence intensity reaches the predetermined threshold, indicating exponential growth. Each experiment was repeated three times. Primer sequences are detailed in Table S2 [33].

Cell culture, transfection, and grouping

Human trophoblast cell line HTR-8/SVneo (TCH-C389, Starfish Biotechnology Co., Ltd.) and human choriocarcinoma cell line BeWo (TCH-C403, Starfish Biotechnology Co., Ltd.) were purchased. The cells were cultured in Dulbecco's Modified Eagle Medium (DMEM, Gibco, Grand Island, NY, USA) supplemented with 10% fetal bovine serum (FBS), 1% penicillin, and 1% streptomycin and then incubated at 37°C in a 5% CO₂ humidified atmosphere. To establish an in vitro PE cell model, HTR-8/SVneo cells were subjected to a hypoxia-reoxygenation (H/R) pattern by incubating them at 2% oxygen for 16 h, followed by 20% oxygen at 37°C.

Further precise transfection experiments were conducted on HTR-8/SVneo and BeWo cell lines. Lipofectamine 2000 (Invitrogen, USA) was used as the transfection reagent. According to the manufacturer's

protocol, molecules such as miR-155 inhibitor (miR212529133043-1-10, Ruibo Biotechnology Co., Ltd.), inhibitor NC (miR2N0000001-1-5, Ruibo Biotechnology Co., Ltd.), sh-PKG1 (50 nM, GenePharma), sh-NC (50 nM, GenePharma), miR-155 mimic (miR112529132545-1-10, Ruibo Biotechnology Co., Ltd.), and mimic NC (miR1N0000001-1-5, Ruibo Biotechnology Co., Ltd.) were introduced into the cells. The transfection process involved mixing the transfection reagent with each transfectant to form complexes capable of effectively entering the cells, which were then added to cells in culture dishes grown to 70–80% confluence to facilitate the efficient uptake and expression of exogenous nucleic acids. Additionally, cells were treated with PDTC (100 μmol/L, S1808, Biyuntian) and an equal amount of DMSO (Shaanxi Yangyuan Biotechnology Co., Ltd.).

For both the HTR-8/SVneo and BeWo cells, they were divided into Control group, H/R group, miR-155 inhibitor group, inhibitor NC group, sh-NC group, sh-PKG1 group, miR-155 inhibitor+sh-NC group, miR-155 inhibitor+sh-PKG1 group, DMSO group, PDTC group, PDTC+mimic NC group, PDTC+miR-155 mimic group [34].

Transwell invasion assay matrigel-coated

Transwell chambers (Corning, New York, USA) were retrieved from a -20 °C freezing environment and thawed at room temperature. Subsequently, 0.5 mL of serum-free culture medium was added to both the chambers and the corresponding 24-well plate, which were then placed in a 37 °C, 5% CO₂ incubator for 2 h. After incubation, all culture media were removed. Cells were collected by trypsinization, washed twice with PBS, and suspended in serum-free DMEM. Subsequently, 600 μL of medium containing 10% FBS was added to the lower chamber, 100 μL of cell suspension was added to the upper chamber, and the cells were further incubated under the same conditions for 24 h. Following the experiment, aspirate the supernatant and remove non-invading cells on the membrane with a cotton swab. Cells that invaded the membrane were fixed with 4% paraformaldehyde for 20 min, and stained with Giemsa staining. Five random fields were selected under a high-power microscope to calculate and capture images of the invading cells [35].

Scratch test

In the scratch migration assay, cells at the logarithmic growth phase were first seeded into a six-well plate to form a monolayer. The following day, the cells were subjected to respective treatments according to the assigned groups and then continued to be cultured at 37 °C with 5% CO₂. A 100 μL sterile pipette tip was used to scratch

the cell monolayer in the six-well plate, followed by removal of the culture medium, washing the cells twice with PBS, and adding serum-free medium for further cultivation. The scratched area was observed under a microscope, and its status at 0 h was used as the control. Subsequently, the plate was returned to the 37 °C incubator with 5% CO₂ for an additional 24 h of cultivation. After the incubation period, cell migration and its changes were once again observed and documented [35].

Western blot

Tissues were homogenized in a mixture containing pre-chilled RIPA lysis buffer (Thermo Scientific, USA, catalog number 89901) and a mixture of 1×protease/phosphatase inhibitor cocktail (Thermo Scientific, USA, catalog number 78442) to obtain 10% (w/v) homogenates. Subsequently, the homogenates were centrifuged at 4 °C and 13,000 rpm for 20 min followed by collection of the supernatant. The protein concentration was determined using the BCA method and equal amounts (30 µg) of denatured protein samples were separated on an SDS–polyacrylamide gel and then transferred onto a polyvinylidene fluoride (PVDF) membrane.

The membranes were blocked with 5% non-fat milk in TBST (Tris-buffered saline with 0.1% Tween 20) for 1 h at room temperature and then incubated with primary antibodies overnight at 4 °C. After washing with TBST, the membranes were incubated with secondary antibodies for 2 h at room temperature. Finally, protein bands were visualized using ECL reagent (catalog number 34580, Thermo Scientific), and the relative protein content was expressed as the grayscale value of the respective protein band normalized to the grayscale value of the GAPDH protein band. The antibodies were listed in Table S3. Densitometry analysis was conducted using ImageJ software (NIH, Bethesda, Maryland, USA). The experiment was repeated three times [36].

EdU experiment

The proliferation of cells was assessed through the EdU experiment using the 5-ethynyl-2'-deoxyuridine labeling/detection kit (BA2007, Shanghai Shangbao Biotechnology Co., Ltd.). In each confocal culture dish containing cells, 200 µL of dilution solution A was added and incubated for 2 h in a cell culture incubator. The cells were washed with PBS buffer, fixed with 4% paraformaldehyde for 30 min, and subsequently decolorized using a 2 mg/mL glycine solution for 5 min on a shaker at room temperature. Following this, 200 µL of 0.5% Triton X-100 was added to each well and incubated at room temperature for 10 min. After a single wash with PBS buffer, 200 µL of pre-prepared 1×Apollo dye was added to each well and incubated in the dark at room temperature for

30 min. Subsequent to two washes with PBS buffer, 0.5% Triton X-100 was introduced to each well for a 10-min incubation. Next, 200 µL of dilution solution F was added to each well and incubated in the dark at room temperature for 30 min, followed by two rinses with PBS buffer. Upon completion of the staining process, the culture dishes were examined under a fluorescence microscope [37].

Flow cytometry analysis

Flow cytometry was utilized to assess the cell death rate (Beckman Coulter, Brea, CA, USA). In brief, cells from each group (1×10^5 cells per well) were collected, washed with chilled PBS, and subsequently stained in the dark using the apoptosis assay kit (APOAF-20TST, Sigma-Aldrich, USA) for 15 min. Afterward, the pellet was resuspended in 400 µL of binding buffer and stained with 5 µL Annexin-V provided in the apoptosis assay kit. Subsequently, the cells were analyzed using the Novocyte flow cytometer (ACEA Biosciences Inc., San Diego, CA, USA) [38].

Fluorescent enzyme reporter gene assay

In this study, we first utilized miRDB to predict the potential binding sites between miR-155 and the PKG1 protein. Based on these predictive data, we designed and synthesized wild-type (wt-PKG1) and mutant-type (mut-PKG1) sequences of PKG1. Subsequently, these sequences were cloned into the fluorescent enzyme reporter vector pGL3-Promoter (VQP0124, Yingrun Biotechnology).

In the experiment, we utilized standard mimics (50 nM) and miR-155 negative control (50 nM, GenePharma). These mimics were co-transfected with the fluorescent enzyme reporter vector into HTR-8/SVneo cells. Upon completion of transfection, we measured the luminescence intensity of each sample using the dual-luciferase reporter gene assay kit provided by Promega to validate the interaction between miR-155 and PKG1.

To ensure the accuracy and reproducibility of the experimental results, we established the following experimental groups and conducted three replicates for each group: mimic+mut-PKG1 group, mimic+wt-PKG1 group, mimic NC (negative control)+mut-PKG1 group, and mimic NC+wt-PKG1 group [28].

RNA pull-down experiment method

In this study, we employed the Pierce Magnetic RNA–Protein Pull-Down assay kit (20,164, Merck) provided by Millipore to conduct the RNA Pull-down experiment. Initially, we biotinylated the PKG1 protein (Geneseed, Guangzhou, China) and incubated it with biotinylated negative controls in lysates of HTR-8/SVneo cells at

room temperature for 2 h. Subsequently, the experiment involved incubation with magnetic beads conjugated with streptavidin at the same temperature for 1 h to capture the complex formed by PKG1 and miR-155. Following the incubation, the mixture was further treated with a buffer containing proteinase K at room temperature for 1 h. Finally, the eluted complex was analyzed through a quantitative reverse transcription-polymerase chain reaction [39].

Statistical analysis methods

Our study utilized R language version 4.2.1 for data processing, with the assistance of the integrated development environment RStudio version 4.2.1 for compilation. Additionally, Perl language version 5.30.0 was employed for file handling, along with Origin statistical software version 2021. Continuous data were expressed as means \pm standard deviations, and between-group comparisons were conducted using an independent samples t-test [40]. Data comparisons between different groups were performed using a one-way analysis of variance, with a significance level set at $p < 0.05$ [41].

Results

Studies on PE model mice and in vitro cell research reveal the pivotal role of miR-155 in the pathogenesis of PE

PE is a multi-organ disease caused by various factors that pose a significant threat to maternal and infant health, yet its etiology and pathogenesis remain incompletely understood. In order to investigate the molecular mechanisms involved in the development of PE, we first established a PE mouse model (Fig. S1A). Compared to the Control group, the PE group exhibited significantly higher systolic and diastolic blood pressure, proteinuria levels, and a notable decrease in the number of fetuses and placentas (Fig. S1B–D). Furthermore, it was observed that compared to the Control group, pregnant mice in the PE group had significantly reduced placental growth factor (PlGF) expression and increased levels of soluble fms-like tyrosine kinase-1 (sFlt-1) and tumor necrosis factor- α (TNF- α) (Fig. S1E). Subsequent evaluation of the morphological changes in maternal kidneys and placentas revealed that compared to the Control group, the PE

group showed signs of glomerular atrophy and narrowing of glomerular spaces in renal tissue, along with more intense blue staining in labyrinth layers of placental tissue in Masson's trichrome staining (Fig. S1F). These results confirm the successful construction of the PE mouse model.

Subsequently, miRNA transcriptomic sequencing was performed on mouse placental tissues, resulting in the identification of 23 significantly differentially expressed miRNAs (Fig. 1A). Validation of the three miRNAs with the greatest differential expression (miR-155, miR-127, and miR-99b) using RT-qPCR revealed that the expression level of miR-155 in PE mouse placental tissues was significantly higher than in the control group, showing the most pronounced difference (Fig. 1B). Therefore, further investigation will focus on elucidating the regulatory mechanisms of miR-155 in the onset and progression of PE.

Building upon this, human trophoblast-derived cell lines HTR-8/SVneo and BeWo were subjected to a H/R model to establish an in vitro PE cell model. Transfection of these cells with a miR-155 inhibitor and subsequent H/R treatment (Fig. 1C) showed that in the H/R group, the expression of miR-155 significantly increased, while transfection with the miR-155 inhibitor markedly reduced the level of miR-155 (Fig. 1D). Transwell and scratch assays indicated that in HTR-8/SVneo cells, H/R treatment decreased the invasive and migratory abilities of the cells, whereas transfection with the miR-155 inhibitor significantly enhanced these capabilities (Fig. 1E–F). Furthermore, compared to the control group, the H/R group exhibited a significant decrease in markers associated with improved invasiveness of the nutritive layer (N-cadherin, vimentin, and Twist) and a notable increase in the inhibitory marker (E-cadherin), which was reversed by transfection with the miR-155 inhibitor (Fig. 1G).

Furthermore, the influence of miR-155 on trophoblast cell proliferation was evaluated through EdU assays. It was found that in HTR-8/SVneo cells, compared to the control group, cell proliferation significantly decreased in the H/R group, but transfection with the miR-155 inhibitor promoted cell proliferation (Fig. 1H). Regarding

(See figure on next page.)

Fig. 1 miR-155 Inhibits the Invasion of Human Trophoblast-Derived Cell Lines HTR-8/SVneo. Note: **A** Heat map showing miRNA transcriptome sequencing in mouse placental tissue; **B** RT-qPCR analysis of the expression levels of miR-155, miR-127, and miR-99b, $n = 6$; **C** Flowchart of cell treatment; **D** RT-qPCR analysis of miR-155 expression in human trophoblast-derived cell lines HTR-8/SVneo and BeWo after H/R treatment; **E** Transwell assay assessing the invasive capability of trophoblast cells HTR-8/SVneo, scale bars = 50 μ m; **F** Scratch assay evaluating the migratory ability of trophoblast cells HTR-8/SVneo, scale bars = 100 μ m; **G** Western Blot analysis of N-cadherin, vimentin, Twist, and E-cadherin expression levels; **H** EdU staining for assessing the proliferative capacity of trophoblast cells HTR-8/SVneo, scale bars = 50 μ m; **I** Flow cytometry analysis of apoptosis in trophoblast cells HTR-8/SVneo. Cell experiments were repeated three times ($n = 3$), * indicates $p < 0.05$ between the two groups

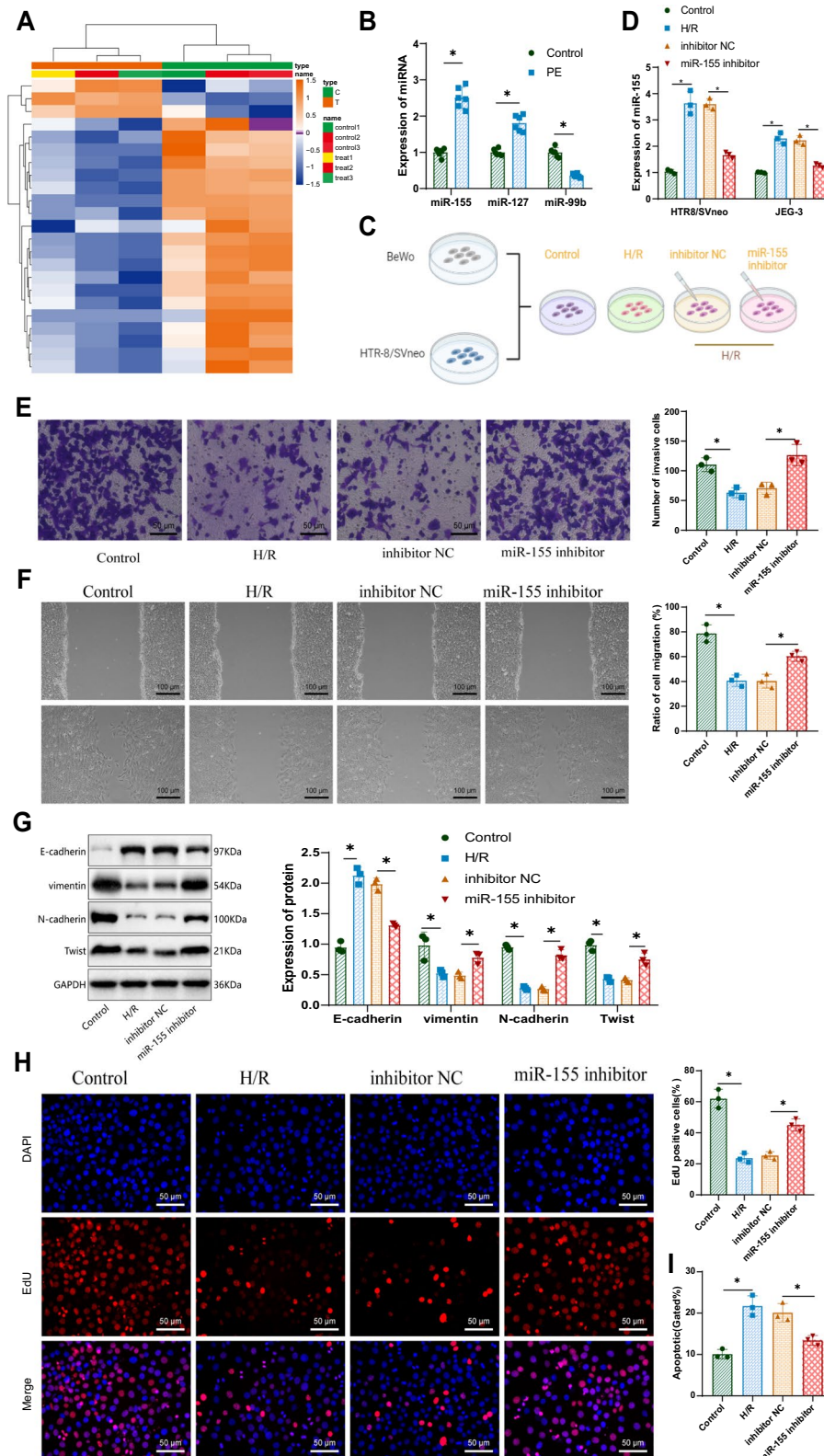


Fig. 1 (See legend on previous page.)

apoptosis, the H/R group exhibited a significantly higher level of apoptosis compared to the control group, which was partially inhibited by transfection with the miR-155 inhibitor (Fig. 1I). Similar results were observed in BeWo cells (Fig. S2A–D). These findings further underscore the pathogenic mechanism in PE involving miR-155 inhibition of trophoblast cell infiltration and promotion of trophoblast cell apoptosis.

MicroRNA-155 regulation of PKG1 in the pathogenesis of PE: mechanistic insights and identification of potential therapeutic targets

To investigate further the molecular mechanisms underlying miR-155 regulation in the progression of PE, we utilized the miRDB database to identify the binding site of miR-155 on PKG1 (Fig. 2A). Through dual-luciferase reporter gene analysis, we observed a significant decrease in luciferase activity in the experimental group containing the wild-type PKG1 sequence in the presence of the

mimic (Fig. 2B), thereby confirming the direct interaction between miR-155 and PKG1. Furthermore, RNA pull-down experiments validated the binding of endogenous miR-155 to biotinylated PKG1 probes (Fig. 2C), strengthening the evidence of the miR-155 and PKG1 interaction.

Subsequent examination of PKG1 expression in placental tissues from PE mice, control group, and H/R-treated HTR-8/SVneo cells was performed using RT-qPCR and Western Blot analysis. The results indicated a significant downregulation of PKG1 expression in placental tissues of PE mice and H/R-treated HTR-8/SVneo cells compared to the control group (Fig. 2D–G). Remarkably, transfection of HTR-8/SVneo cells with a miR-155 inhibitor followed by exposure to H/R conditions led to a significant upregulation of PKG1 expression as demonstrated by RT-qPCR and Western Blot analyses (Fig. 2H–I). Similar findings were observed in BeWo cells (Fig. 2J–M). These discoveries not only unveil the potential role of miR-155 in regulating PKG1 during PE

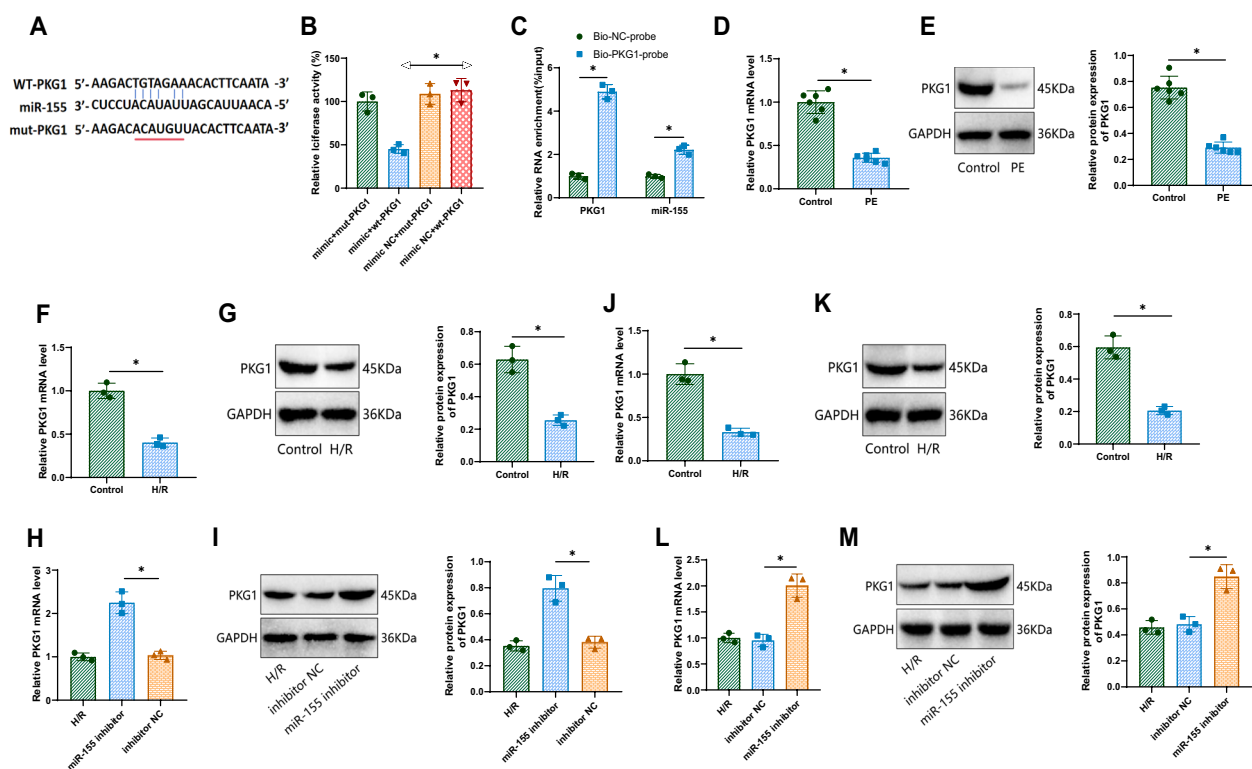


Fig. 2 miR-155 promotes apoptosis in human trophoblast-derived cell lines. Note: **A** Prediction of the binding sites of PKG1 and miR-155 from the miRDB website; **B** Confirmation of the interaction between PKG1 and miR-155 by dual-luciferase reporter gene assay; **C** Validation of the interaction between PKG1 and miR-155 through RNA pull-down analysis; **D** Detection of PKG1 mRNA expression in mouse placental tissues by RT-qPCR; **E** Evaluation of PKG1 protein expression in mouse placental tissues by Western Blot, $n=6$; **F** Measurement of PKG1 mRNA expression in H/R-treated HTR-8/SVneo cells by RT-qPCR; **G** Analysis of PKG1 protein expression in H/R-treated HTR-8/SVneo cells by Western Blot; **H** Assessment of PKG1 mRNA expression in HTR-8/SVneo cells transfected with miR-155 inhibitor by RT-qPCR; **I** Determination of PKG1 protein expression in HTR-8/SVneo cells transfected with miR-155 inhibitor by Western Blot; **J** Quantification of PKG1 mRNA expression in H/R-treated BeWo cells by RT-qPCR; **K** Examination of PKG1 protein expression in H/R-treated BeWo cells by Western Blot; **L** Measurement of PKG1 mRNA expression in BeWo cells transfected with miR-155 inhibitor by RT-qPCR; **M** Analysis of PKG1 protein expression in BeWo cells transfected with miR-155 inhibitor by Western Blot. Cell experiments were repeated three times ($n=3$). * indicates a statistical significance of $p < 0.05$ between the two groups

development but also provide crucial molecular targets for future therapeutic strategies.

The mechanism and impact of miR-155 regulation of PE trophoblast cell function via targeting PKG1

In order to gain a deeper understanding of the impact of miR-155 on PE trophoblast cell function, particularly elucidating how it functions through targeting PKG1, we transfected HTR-8/SVneo cells with sh-PKG1 and a miR-155 inhibitor, followed by exposure to H/R conditions (Fig. 3A). Results from RT-qPCR and Western Blot analyses revealed that silencing PKG1 led to a decrease in intracellular levels of both PKG1 mRNA and protein. Comparing cells co-transfected with the miR-155 inhibitor and sh-PKG1 to cells transfected solely with the miR-155 inhibitor, a significant decrease in PKG1 expression levels was observed (Fig. 3B–C).

Furthermore, findings from Transwell and scratch assays demonstrated that sh-PKG1 effectively reversed the enhanced invasive and migratory capabilities of HTR-8/SVneo cells induced by the miR-155 inhibitor (Fig. 3D–E). At the protein level, cells co-transfected with both sh-PKG1 and the miR-155 inhibitor exhibited marked reductions in the expression of N-cadherin, vimentin, and Twist, while E-cadherin expression increased compared to cells transfected only with the miR-155 inhibitor (Fig. 3F).

Moreover, compared to the sh-NC group, cells treated with sh-PKG1 displayed significantly reduced proliferation and notably increased apoptosis levels. Co-transfection of the miR-155 inhibitor and sh-PKG1 resulted in a further decrease in proliferation and a significant increase in apoptosis compared to cells transfected solely with the miR-155 inhibitor (Fig. 3G–H). Similar patterns were observed in BeWo cells, corroborating our findings and suggesting the reproducibility of these effects across different trophoblast-derived cell lines (Fig. S3A–F). These results highlight the central role of miR-155 in inhibiting PE-related trophoblast cell invasion, migration, proliferation, and promoting apoptosis, revealing its execution of these functions through modulation of PKG1 expression.

NF- κ B promotes miR-155 impact on trophoblast cell viability

The study revealed that NF- κ B can promote the involvement of miR-155 in inflammatory responses [42]. To gain a deeper understanding of the molecular mechanism by which miR-155 regulates PE trophoblast cells, we conducted analyses using RT-qPCR and Western Blot. Our observations in mouse placental tissues affected by PE and in HTR-8/SVneo cells subjected to H/R treatment showed no difference in the expression levels of NF- κ B p65, while the expression of p-NF- κ B p65 was significantly higher than in the control group. This result highlights the importance of NF- κ B activation under pathological conditions (4A–D).

In further experiments, we treated trophoblast cells with the NF- κ B inhibitor PDTC and simulated its biological effects by transfecting with miR-155 mimic (Fig. 4E). The results of the analysis indicated that inhibiting NF- κ B not only decreased the expression of miR-155 but also increased the level of PKG1. Transfection with miR-155 mimic reversed the effects of PDTC, enhancing the expression of miR-155 and suppressing the level of PKG1 (Fig. 4F–G).

Regarding cell invasion and migration, results from Transwell and scratch tests showed that cells treated with PDTC exhibited significantly enhanced invasion and migration abilities compared to the DMSO control group. In contrast, the PDTC+miR-155 mimic group displayed weakened invasion and migration capabilities compared to the PDTC+mimic NC group. At the protein level, PDTC treatment significantly increased the expression of N-cadherin, vimentin, and Twist while reducing E-cadherin expression. Conversely, compared to the PDTC+mimic NC group, the PDTC+miR-155 mimic-treated cells showed reduced expression of N-cadherin, vimentin, and Twist and increased expression of E-cadherin (Fig. 4H–J).

Furthermore, trophoblast cells treated with PDTC showed significantly increased proliferative capacity and markedly decreased apoptosis levels compared to the DMSO control group. When cells were transfected with miR-155 mimic, the PDTC+miR-155 mimic group exhibited a decrease in proliferative capacity and

(See figure on next page.)

Fig. 3 Evaluation of the Growth Status of Trophoblast Cell Line HTR-8/SVneo. Note: **A** Schematic of cell transfection process; **B** RT-qPCR analysis of PKG1 mRNA expression levels in different groups of HTR-8/SVneo cells; **C** Western Blot assessment of PKG1 protein expression levels in various groups of HTR-8/SVneo cells; **D** Transwell assay measuring the invasive capacity of trophoblast cell line HTR-8/SVneo, scale bars = 50 μ m; **E** Scratch assay evaluating the migratory capability of trophoblast cells HTR-8/SVneo, scale bars = 100 μ m; **F** Western Blot analysis of N-cadherin, vimentin, Twist, and E-cadherin expression levels; **G** EDU staining for assessing the proliferative ability of trophoblast cells HTR-8/SVneo, scale bars = 50 μ m; **H** Flow cytometry analysis of apoptosis in trophoblast cells HTR-8/SVneo. Cell experiments were repeated three times ($n = 3$), * indicates $p < 0.05$ between the two groups

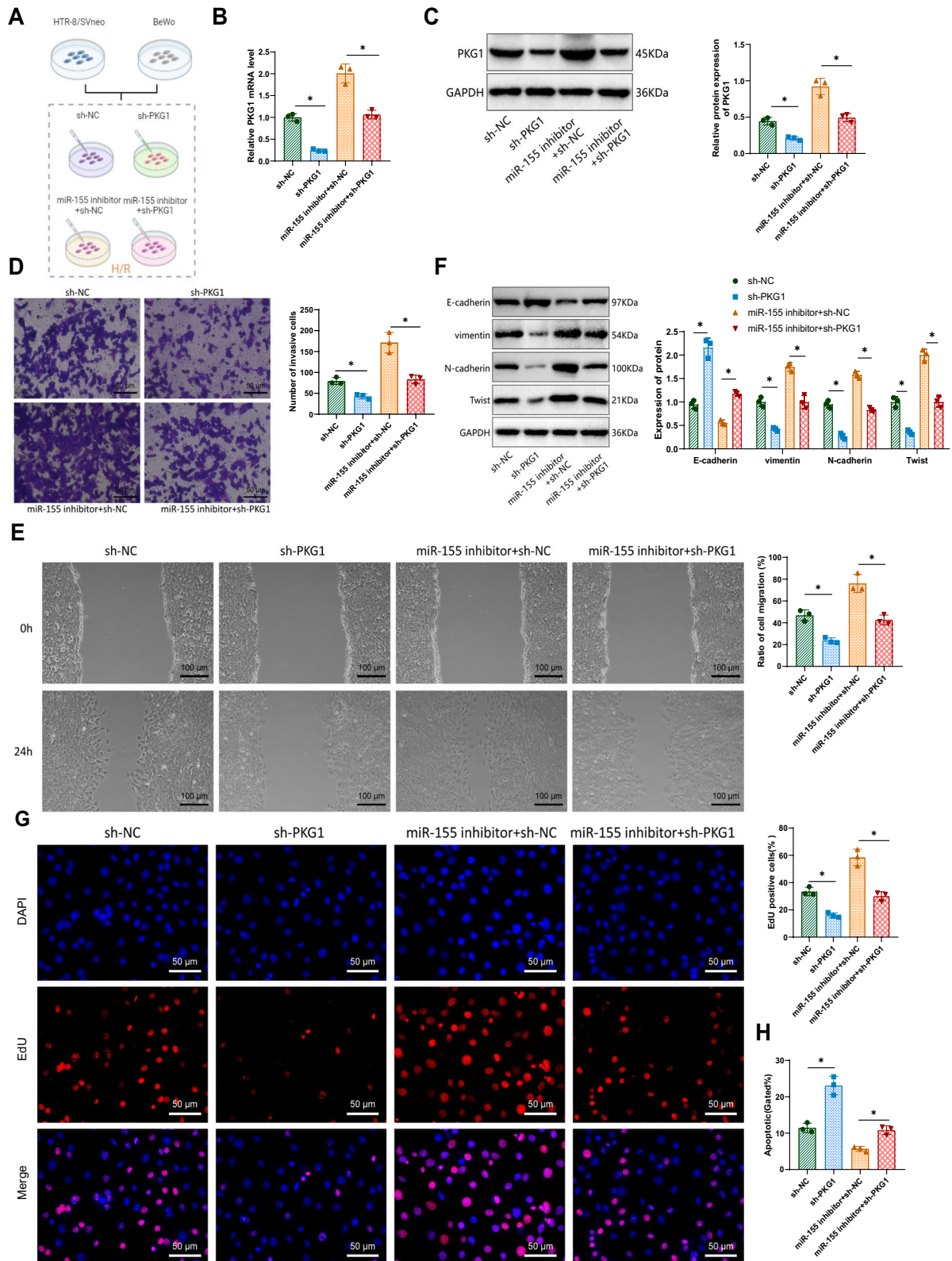


Fig. 3 (See legend on previous page.)

a significant increase in apoptosis rate compared to the PDTc+mimic NC group (Fig. 4K–L). Similar trends were observed in the BeWo cell line, further reinforcing our findings and indicating that NF- κ B and miR-155 play consistent and reproducible roles in regulating proliferation and apoptosis in trophoblast cells (Fig. S4A–H). These findings further confirm that NF- κ B regulates invasion, migration, proliferation, and apoptosis in PE trophoblast cells through miR-155.

In vivo validation of miR-155 targeting PKG1 in promoting the PE process

To investigate the regulatory mechanism of miR-155 targeting PKG1 in the PE process, we established a successful mouse model of PE and locally injected placental tissues to explore the impact of miR-155 targeting PKG1 on the pathogenesis of PE (Fig. 5A). We observed that silencing PKG1 not only resulted in elevated blood pressure and increased proteinuria levels in preeclamptic mice but also significantly decreased the number of fetuses and placentas. In preeclamptic mice treated with a combination of miR-155 antagomir and sh-PKG1, compared to those treated with miR-155 antagomir alone, higher blood pressure and proteinuria levels, as well as a lower number of fetuses and placentas, were observed, suggesting that miR-155 targeting PKG1 might exacerbate the symptoms of PE (Fig. 5B–D).

Further analysis revealed that compared to the sh-NC group, pregnant mice treated with sh-PKG1 showed a significant decrease in Placental Growth Factor (PlGF) expression and a marked increase in soluble fms-like tyrosine kinase-1 (sFlt-1) and tumor necrosis factor- α (TNF- α) expression. When miR-155 antagomir and sh-PKG1 were used in combination, preeclamptic mice exhibited a further reduction in PlGF expression and increased expression of sFlt-1 and TNF- α compared to using miR-155 antagomir alone (Fig. 5E–G).

Further investigations revealed that transfection of miR-155 antagomir reduced miR-155 levels, whereas silencing PKG1 did not affect miR-155 expression (Fig. 6A). Additionally, the co-administration of miR-155

antagomir and sh-PKG1 led to an increase in PKG1 expression in preeclamptic mice compared to using sh-PKG1 alone (Fig. 6B–C). Morphological changes in maternal kidneys and placental tissues were assessed. Mice treated with sh-PKG1 exhibited more severe kidney damage, including glomerular atrophy and narrowed cyst cavities, in contrast to the sh-NC group. In placental tissues, denser blue staining under Masson's trichrome stain indicated pathological changes in the labyrinth layer. Combinatorial treatment of miR-155 antagomir and sh-PKG1 showed more pronounced morphological damage in kidneys and placentas in mice compared to miR-155 antagomir + sh-NC treatment (Fig. 6D). At the protein level, pregnant mice treated with sh-PKG1 displayed reduced expression of N-cadherin, vimentin, and Twist and increased expression of E-cadherin compared to the sh-NC group. Moreover, the combined treatment of miR-155 antagomir and sh-PKG1 showed a decreasing trend in N-cadherin, vimentin, and Twist expression and an increase in E-cadherin expression in mice compared to miR-155 antagomir + sh-NC treatment (Fig. 6E). Overall, these findings elucidate the potential role of miR-155 targeting PKG1 in exacerbating the progression of PE, highlighting the beneficial role of PKG1 in maintaining pregnancy balance and laying a foundation for potential future therapeutic targets.

Discussion

miR-155's regulation of PKG1 in PE has been a subject of significant interest. This study, through in-depth experiments and analysis, reveals the critical role of miR-155 and PKG1 in the pathogenesis of PE. In contrast to prior research, our study systematically investigates the direct regulatory relationship between miR-155 and PKG1, confirming miR-155's negative regulatory effect on PKG1 through in vivo and in vitro experiments. This discovery provides new evidence for understanding the role of miR-155 in the pathogenesis of PE and establishes an experimental foundation for the potential therapeutic targeting of miR-155 [11, 13, 43].

(See figure on next page.)

Fig. 4 Evaluation of the Growth Status of Trophoblast Cell Line HTR-8/SVneo. Note: **A** RT-qPCR analysis of NF- κ B p65 mRNA expression levels in mouse placental tissues from various groups; **B** Western Blot assessment of NF- κ B p65 and p-NF- κ B p65 protein expression levels in mouse placental tissues from different groups; **C** RT-qPCR analysis of NF- κ B p65 mRNA expression levels in H/R-treated HTR-8/SVneo cells; **D** Western Blot analysis of NF- κ B p65 and p-NF- κ B p65 protein expression levels in H/R-treated HTR-8/SVneo cells; **E** Schematic of cell transfection process; **F** RT-qPCR analysis of NF- κ B p65 mRNA, PKG1 mRNA, and miR-155 expression levels in H/R-treated HTR-8/SVneo cells; **G** Western Blot assessment of NF- κ B p65, p-NF- κ B p65, and PKG1 protein levels in different cell groups; **H** Transwell assay to measure the invasive capacity of trophoblast cell line HTR-8/SVneo, scale bars = 50 μ m; **I** Scratch assay evaluating the migratory ability of trophoblast cells HTR-8/SVneo, scale bars = 100 μ m; **J** Western Blot analysis of N-cadherin, vimentin, Twist, and E-cadherin expression levels; **K** EDU staining for assessing the proliferative capacity of trophoblast cells HTR-8/SVneo, scale bars = 50 μ m; **L** Flow cytometry analysis of apoptosis in trophoblast cells HTR-8/SVneo. Cell experiments were repeated three times (n = 3), * indicates $p < 0.05$ between the two groups

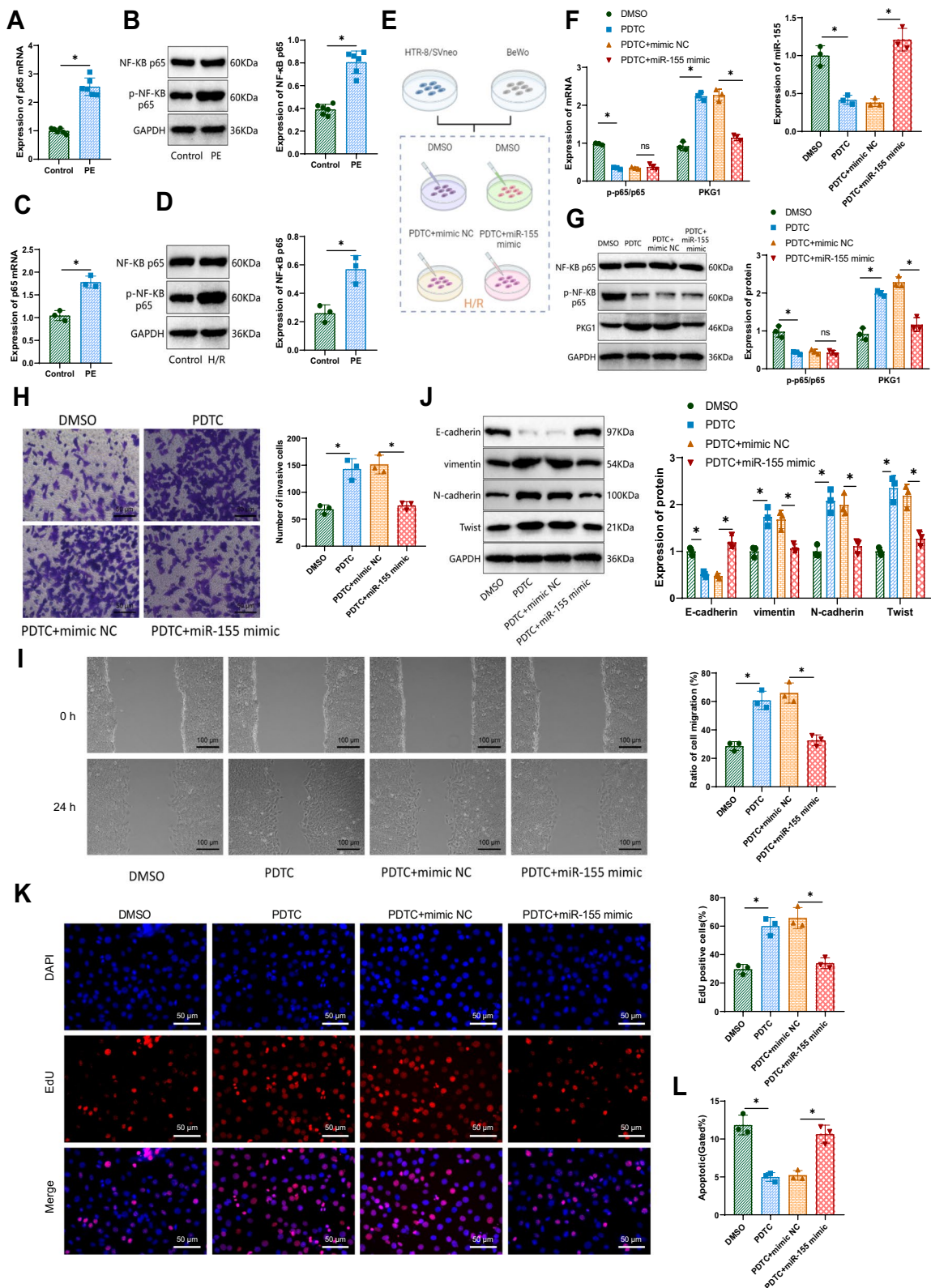


Fig. 4 (See legend on previous page.)

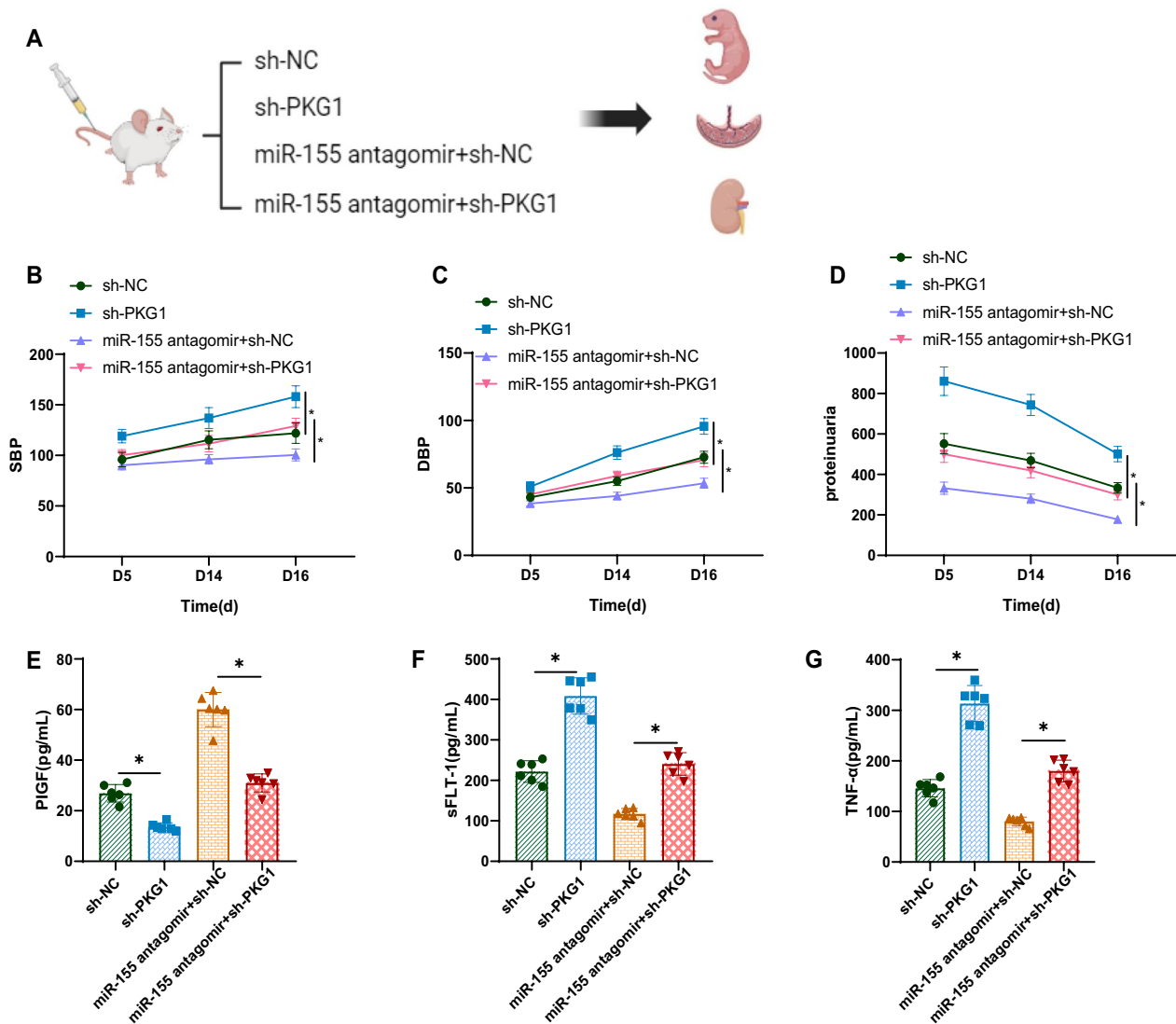


Fig. 5 Assessment of PE Indices in Mice. Note: **A** Schematic of model construction; **B** Measurement of systolic blood pressure (SBP) in mice from various groups; **C** Measurement of diastolic blood pressure (DBP) in mice from different groups; **D** Evaluation of proteinuria levels in mice of each group; **E–G** ELISA analysis of PIGF, sFlt-1, and TNF- α plasma levels in pregnant mice of different groups. $n=6$, * indicates $p < 0.05$ between the two groups

The mutual regulation mechanism between miR-155 and NF- κ B in the pathogenesis of PE is another important finding of this study. Compared to previous studies, our research delves into NF- κ B's regulatory role in miR-155 expression, revealing that the NF- κ B inhibitor PDTC can modulate cell functions by regulating the expression levels of miR-155 and PKG1. This finding expands the understanding of NF- κ B's role in the pathogenesis of PE and provides new directions for future research [44, 45].

The study focuses on the mechanisms of miR-155 and PKG1 in regulating cellular behaviors. In contrast to prior studies, we experimentally confirm through the

Cell signaling pathway that miR-155 inhibition affects cell invasion, migration, and proliferation and further demonstrate that miR-155 inhibition can reverse the pathological manifestations of PE cells. These results deepen the understanding of the interaction mechanisms between miR-155 and PKG1 in regulating cellular behaviors and offer new insights for the treatment of related diseases [17].

The biological effects of NF- κ B in the pathogenesis of PE are another significant aspect of this study. We discovered NF- κ B activation in PE and further experimentally validated the regulatory effects of the NF- κ B inhibitor

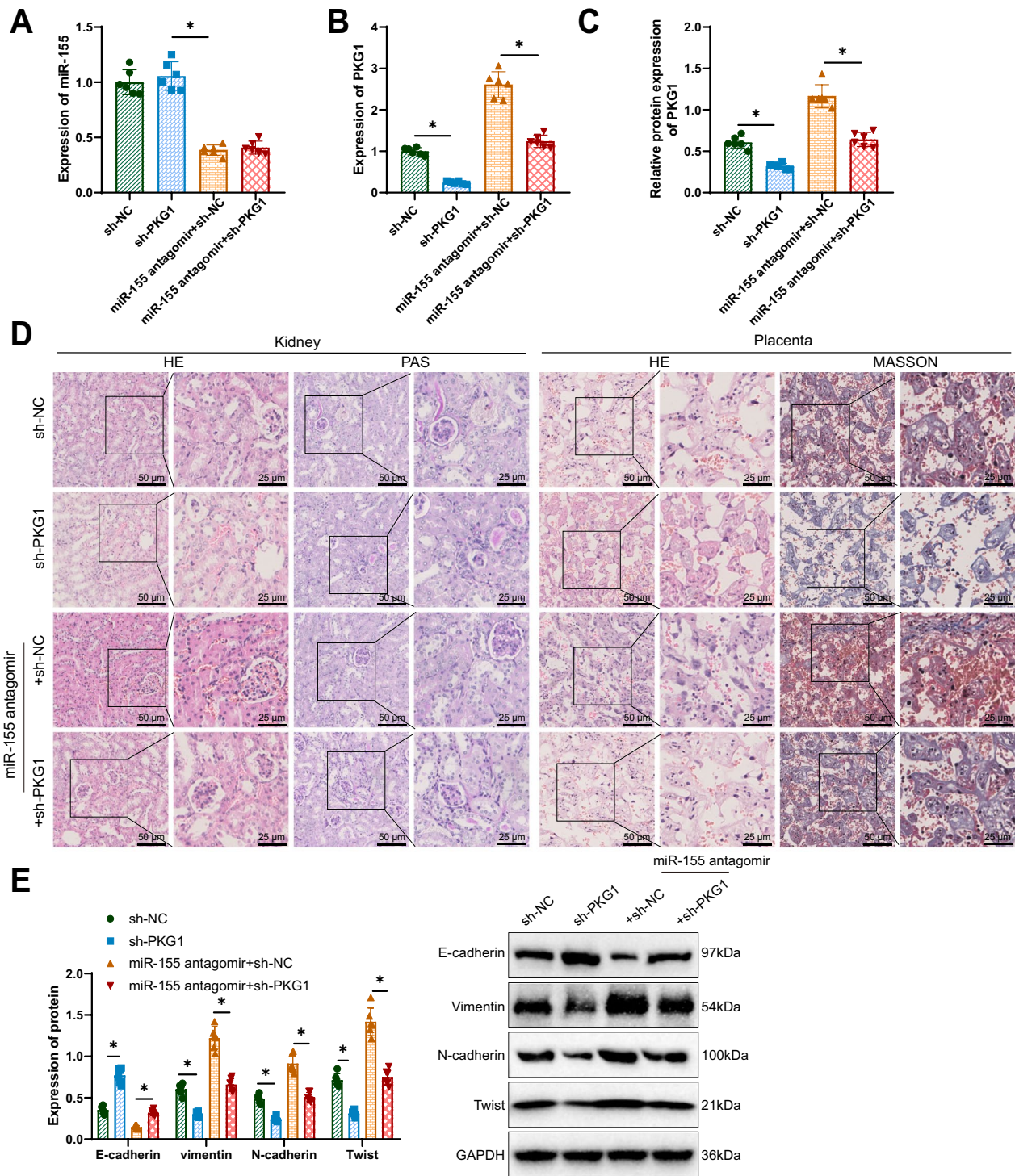


Fig. 6 Investigating the Role of miR-155 Targeting PKG1 in Promoting the Progression of PE. Note: **A** RT-qPCR analysis of miR-155 expression levels in embryo tissues from different groups; **B** RT-qPCR assessment of PKG1 mRNA expression levels in embryo tissues from various groups; **C** Western Blot analysis of PKG1 protein expression levels in embryo tissues from different groups; **D** Representative HE and PAS staining images of kidney sections from pregnant mice in each group, and typical HE and MASSON staining images of placental sections from pregnant mice, scale bars = 50/25 μm; **E** Western Blot analysis of N-cadherin, vimentin, Twist, and E-cadherin expression levels. n = 6, * indicates $p < 0.05$ between the two groups

PDTC on miR-155 and PKG1. Unlike prior studies, our research confirms the impact of NF- κ B activation on miR-155 expression levels, thereby influencing the functional state of cells. This result deepens the understanding of NF- κ B's critical role in the pathogenesis of PE.

The innovation of this study lies in the comprehensive investigation of the crucial regulatory mechanisms of miR-155 and PKG1 in PE while also revealing the significant role of NF- κ B in this process. These research findings not only enhance the understanding of the pathophysiology of PE but also provide a theoretical basis for the development of novel therapeutic strategies and drugs. They hold important scientific and clinical application value, with potential prospects in future research and clinical practice.

However, this study also faces some limitations, such as a small sample size and room for improvement in experimental design. It is necessary to refine the experimental design further, expand the sample size, and validate the stability and reproducibility of the experimental results in future studies. Additionally, future research could delve into the expression levels of miR-155 and PKG1 in different populations and their clinical implications to provide stronger support for personalized therapy.

Overall, the experimental design and interpretation of results in this study provide compelling evidence for elucidating the roles of miR-155 and PKG1 in the pathogenesis of PE. This study offers new insights and a theoretical foundation for therapeutic strategies and drug development for PE, bearing significant scientific and clinical implications. Looking ahead, further research can delve deeper into the regulatory mechanisms of miR-155,

PKG1, and NF- κ B to lay the groundwork for a better understanding of the mechanisms underlying PE and the development of more effective treatment strategies.

Conclusion

In this study, we delved into the role of miR-155 in the pathogenesis of PE, specifically its regulatory impact on cGMP-dependent protein kinase I (PKG1). Our experimental findings demonstrate a significant upregulation of miR-155 expression in a PE mouse model. This discovery is crucial for understanding the molecular mechanisms of PE, as alterations in miR-155 directly affect the invasive, migratory, proliferative, and apoptotic abilities of trophoblast cells. By inhibiting miR-155 expression, we observed a notable improvement in trophoblast cell function, further confirming the critical role of miR-155 in the pathogenesis of PE (Fig. 7).

Furthermore, our research revealed the importance of the NF- κ B pathway in regulating miR-155 expression. NF- κ B, as a key cytokine, plays a vital role in controlling gene expression in various pathological processes. Under PE conditions, NF- κ B activation may be one of the primary mechanisms leading to the upregulation of miR-155 expression. This finding not only presents a new molecular target for PE but also paves the way for future therapeutic strategies.

However, our study has several limitations. For example, while we validated the targeting relationship between miR-155 and PKG1, the specific biological functions and mechanisms of PKG1 in PE remain unclear. Future research should delve deeper into exploring the role of PKG1 in the pathogenesis of PE and how it is regulated

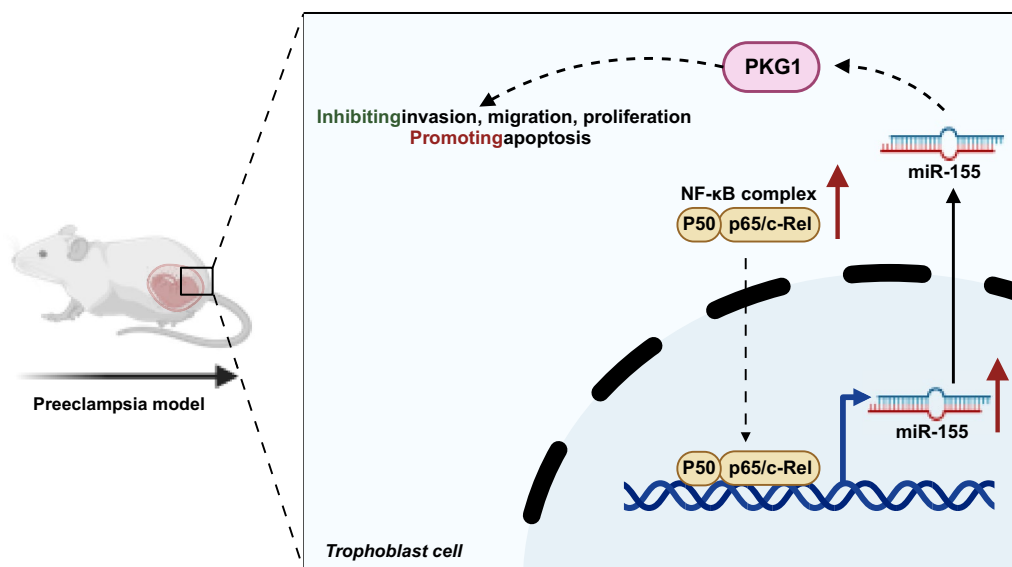


Fig. 7 The Molecular Mechanism of NF- κ B-Mediated miR-155 Targeting PKG1 in Influencing the Progression of PE

by miR-155. Given the complexity of PE and the involvement of numerous factors, studying other potential molecules and signaling pathways is equally important.

In conclusion, our study provides new insights into the intricate molecular mechanisms of PE and a scientific basis for developing therapeutic strategies based on miR-155. We hope that these discoveries will lay the foundation for future clinical research and ultimately improve the treatment outcomes of PE patients by targeting miR-155 and its related pathways. With ongoing research uncovering more about the molecular mechanisms of PE, we look forward to developing more effective prevention and treatment strategies to enhance maternal and infant health globally.

Supplementary Information

The online version contains supplementary material available at <https://doi.org/10.1186/s13062-024-00526-6>.

Supplementary Material 1: Figure S1. Construction of the PE Model. Note: (A) Modeling scheme of the LPS-induced PE mouse model; (B) Measurement of systolic blood pressure (SBP) in mice from different groups; (C) Measurement of diastolic blood pressure (DBP) in mice from various groups; (D) Evaluation of proteinuria levels in mice from each group; (E) ELISA analysis of PIGF, sFlt-1, and TNF- α plasma levels in pregnant mice from different groups; (F) Representative HE and PAS staining images of kidney sections from pregnant mice in each group, and typical HE and MASSON staining images of placental sections from pregnant mice, scale bars=50 μ m. n=6, * indicates $p < 0.05$ between the two groups.

Supplementary Material 2: Figure S2. Inhibition of Growth in Human Trophoblast-Derived Cell Line BeWo by miR-155. Note: (A) Transwell assay assessing the invasive capacity of trophoblast cell BeWo, scale bars=50 μ m; (B) Scratch assay evaluating the migratory ability of trophoblast cell BeWo, scale bars=100 μ m; (C) Western Blot analysis of N-cadherin, vimentin, Twist, and E-cadherin expression levels; (D) EDU staining to evaluate the proliferative capacity of trophoblast cell BeWo, scale bars=50 μ m; (E) Flow cytometry analysis of apoptosis in trophoblast cell BeWo; Cell experiments were repeated three times (n = 3), * indicates $p < 0.05$ between the two groups.

Supplementary Material 3: Figure S3. Evaluation of Growth in Trophoblast Cell Line BeWo. Note: (A) RT-qPCR analysis of PKG1 mRNA expression levels in BeWo cells from different groups; (B) Western Blot assessment of PKG1 protein expression levels in BeWo cells from various groups; (C) Transwell assay to measure the invasive capacity of trophoblast cell BeWo, scale bars=50 μ m; (D) Scratch assay assessing the migratory ability of trophoblast cell BeWo, scale bars=100 μ m; (E) Western Blot analysis of N-cadherin, vimentin, Twist, and E-cadherin expression levels; (F) EDU staining for assessing the proliferative capacity of trophoblast cell HTR-8/SVneo, scale bars=50 μ m; (G) Flow cytometry analysis of apoptosis in trophoblast cell BeWo. Cell experiments were repeated three times (n = 3), * indicates $p < 0.05$ between the two groups.

Supplementary Material 4: Figure S4. Trophoblast Cell Growth in BeWo Cell Line. Note: (A) Detection of NF- κ B p65 mRNA, PKG1 mRNA, and miR-155 expression levels in BeWo cells treated with H/R using RT-qPCR. (B) Evaluation of NF- κ B p65, p-NF- κ B p65 protein expression levels, and PKG1 protein levels in various cell groups using Western Blot. (C) Assessment of the invasive capacity of trophoblast cells BeWo using Transwell, with scale bars set at 50 μ m. (D) Migration capability of trophoblast cells BeWo measured through scratch assays, with scale bars set at 100 μ m. (E) Expression levels of N-cadherin, vimentin, Twist, and E-cadherin detected by Western Blot. (F) The proliferation capability of trophoblast cells HTR-8/SVneo was examined using EDU staining, with scale bars set at 50 μ m. (G) The apoptosis status of trophoblast cells HTR-8/SVneo was analyzed through flow

cytometry. Cell experiments were repeated three times (n = 3), * indicates $P < 0.05$ between the two groups.

Supplementary Material 5.

Acknowledgements

None.

Author contributions

Ningning Chen, Xiaohua Luo, and Xiaopei Guo conceived and designed the study. Rui Peng, Ci Pan, and Zhuyin Li performed the experiments. Bing Zhao, Ruonan Ji, and Siyu Li analyzed the data. Ningning Chen and Xiaohua Luo wrote the manuscript. All authors reviewed and approved the final version of the manuscript.

Funding

This study was supported by Provincial and Ministry Joint Key Project of Medical Science and Technology Tackling Programme of Henan Province in 2023 by Henan Provincial Health and Health Commission (SBGJ202302083).

Availability of data and materials

No datasets were generated or analysed during the current study.

Declarations

Ethics approval and consent to participate

The animal experiments in this study strictly adhered to international and national ethical guidelines and regulations concerning animal research, ensuring respect and protection for the animals. The use of experimental animals was approved by the ethics committee (Approval No: 2023-231-01), and all procedures were conducted according to laboratory animal experimental protocols to minimize animal distress and suffering.

Competing interests

The authors declare no competing interests.

Received: 30 June 2024 Accepted: 2 September 2024

Published online: 26 November 2024

References

- Shrestha DB, Budhathoki P, Malbul K, et al. Prevalence, risk factors and outcome of pregnancy induced hypertension in Nepal: a meta-analysis of prevalence studies. *J Nepal Health Res Counc.* 2021;19(2):221–9. <https://doi.org/10.33314/jnhrc.v19i2.3589>.
- Abdelrahim SK, Ahmed ABA, Sharif ME, Adam I. Association between maternal serum 25-hydroxyvitamin D concentrations and the risk of preeclampsia in central Sudan: a case-control study. *Trans R Soc Trop Med Hyg.* 2022;116(5):487–91. <https://doi.org/10.1093/trstmh/traab163>.
- Tossetta G, Fantone S, Piani F, et al. Modulation of NRF2/KEAP1 signaling in preeclampsia. *Cells.* 2023;12(11):1545. <https://doi.org/10.3390/cells12111545>.
- Fantone S, Ermini L, Piani F, et al. Downregulation of argininosuccinate synthase 1 (ASS1) is associated with hypoxia in placental development. *Hum Cell.* 2023;36(3):1190–8. <https://doi.org/10.1007/s13577-023-00901-x>.
- Giannubilo SR, Marzioni D, Tossetta G, Montironi R, Meccariello ML, Ciavattini A. The "Bad Father": paternal role in biology of pregnancy and in birth outcome. *Biology (Basel).* 2024;13(3):165. <https://doi.org/10.3390/biology13030165>.
- Gesuita R, Licini C, Picchiassi E, et al. Association between first trimester plasma htra1 level and subsequent preeclampsia: A possible early marker? *Pregnancy Hypertens.* 2019;18:58–62. <https://doi.org/10.1016/j.preghy.2019.08.005>.
- Liu X, Fei H, Yang C, et al. Trophoblast-derived extracellular vesicles promote preeclampsia by regulating macrophage polarization. *Hypertension.*

- 2022;79(10):2274–87. <https://doi.org/10.1161/HYPERTENSIONAHA.122.19244>.
8. Liao T, Xu X, Ye X, Yan J. DJ-1 upregulates the Nrf2/GPX4 signal pathway to inhibit trophoblast ferroptosis in the pathogenesis of preeclampsia. *Sci Rep*. 2022;12(1):2934. <https://doi.org/10.1038/s41598-022-07065-y>.
 9. Wu G, Meininger CJ, McNeal CJ, Bazer FW, Rhoads JM. Role of L-arginine in nitric oxide synthesis and health in humans. *Adv Exp Med Biol*. 2021;1332:167–87. https://doi.org/10.1007/978-3-030-74180-8_10.
 10. Chamberlain F, Grammatopoulos D. Methodology for isolation of miRNA from the serum of women investigated for pre-eclampsia. *Cureus*. 2023;15(9):e46181. <https://doi.org/10.7759/cureus.46181>.
 11. Wu Q, Ying X, Yu W, et al. Identification of ferroptosis-related genes in syncytiotrophoblast-derived extracellular vesicles of preeclampsia. *Medicine (Baltimore)*. 2022;101(44):e31583. <https://doi.org/10.1097/MD.00000000000031583>.
 12. Scărlătescu AI, Bărbălată T, Sima AV, Stancu C, Niculescu LŞ, Micheu MM. miR-146a-5p, miR-223-3p and miR-142-3p as potential predictors of major adverse cardiac events in young patients with acute ST elevation myocardial infarction-added value over left ventricular myocardial work indices. *Diagnostics (Basel)*. 2022;12(8):1946. <https://doi.org/10.3390/diagnostics12081946>.
 13. Luo X, Pan C, Guo X, et al. Methylation mediated silencing of miR-155 suppresses the development of preeclampsia in vitro and in vivo by targeting FOXO3. *Mediators Inflamm*. 2022;2022:4250621. <https://doi.org/10.1155/2022/4250621>.
 14. Liu Y, Zhao X, Li J, et al. miR-155 inhibits TP53INP1 expression leading to enhanced glycolysis of psoriatic mesenchymal stem cells. *J Dermatol Sci*. 2022;105(3):142–51. <https://doi.org/10.1016/j.jdermsci.2022.02.001>.
 15. Safarzadeh M, Mohammadi-Yeganeh S, Ghorbani-Bidkorbeh F, Haji Molla Hoseini M. Chitosan based nanof ormulation expressing miR-155 as a promising adjuvant to enhance Th1-biased immune responses. *Life Sci*. 2022;297:120459. <https://doi.org/10.1016/j.lfs.2022.120459>.
 16. Schall N, Garcia JJ, Kalyanaraman H, et al. Protein kinase G1 regulates bone regeneration and rescues diabetic fracture healing. *JCI Insight*. 2020;5(9):e135355. <https://doi.org/10.1172/jci.insight.135355>.
 17. Choi S, Park M, Kim J, et al. TNF- α elicits phenotypic and functional alterations of vascular smooth muscle cells by miR-155-5p-dependent down-regulation of cGMP-dependent kinase 1. *J Biol Chem*. 2018;293(38):14812–22. <https://doi.org/10.1074/jbc.RA118.004220>.
 18. Ahmed U, Khaliq S, Ahmad HU, et al. Pathogenesis of diabetic cardiomyopathy and Role of miRNA. *Crit Rev Eukaryot Gene Expr*. 2021;31(1):79–92. <https://doi.org/10.1615/CritRevEukaryotGeneExpr.2021037533>.
 19. Ghafouri-Fard S, Azimi T, Taheri M. Myocardial infarction associated transcript (MIAT): review of its impact in the tumorigenesis. *Biomed Pharmacother*. 2021;133:11040. <https://doi.org/10.1016/j.biopha.2020.111040>.
 20. Capece D, Verzella D, Flati I, Arboretto P, Cornice J, Franzoso G. NF- κ B: blending metabolism, immunity, and inflammation. *Trends Immunol*. 2022;43(9):757–75. <https://doi.org/10.1016/j.it.2022.07.004>.
 21. Zhang GZ, Liu MQ, Chen HW, et al. NF- κ B signalling pathways in nucleus pulposus cell function and intervertebral disc degeneration. *Cell Prolif*. 2021;54(7):e13057. <https://doi.org/10.1111/cpr.13057>.
 22. Kasti AN, Nikolaki MD, Synodinou KD, et al. The effects of stevia consumption on gut bacteria: friend or foe? *Microorganisms*. 2022;10(4):744. <https://doi.org/10.3390/microorganisms10040744>.
 23. Zhao Y, Zong F. Inhibiting USP14 ameliorates inflammatory responses in trophoblast cells by suppressing MAPK/NF- κ B signaling. *Immun Inflamm Dis*. 2021;9(3):1016–24. <https://doi.org/10.1002/iid3.465>.
 24. Villalobos-Labra R, Liu R, Spaans F, et al. Placenta-derived extracellular vesicles from preeclamptic and healthy pregnancies impair ex vivo vascular endothelial function. *Biosci Rep*. 2022;42(12):BSR20222185. <https://doi.org/10.1042/BSR20222185>.
 25. Cotechini T, Komisarenko M, Sperou A, Macdonald-Goodfellow S, Adams MA, Graham CH. Inflammation in rat pregnancy inhibits spiral artery remodeling leading to fetal growth restriction and features of preeclampsia. *J Exp Med*. 2014;211(1):165–79. <https://doi.org/10.1084/jem.20130295>.
 26. Chen Y, Ou Z, Pang M, et al. Extracellular vesicles derived from Akkermansia muciniphila promote placentation and mitigate preeclampsia in a mouse model. *J Extracell Vesicles*. 2023;12(5):e12328. <https://doi.org/10.1002/jev2.12328>.
 27. Liu Y, Zhai R, Tong J, et al. Angiotensin 1–7 and its analogue decrease blood pressure but aggravate renal damage in preeclamptic mice. *Exp Anim*. 2022;71(4):519–28. <https://doi.org/10.1538/expanim.22-0029>.
 28. Gu X, Sun X, Yu Y, Li L. miR-218-5p promotes trophoblast infiltration and inhibits endoplasmic reticulum/oxidative stress by reducing UBE3A-mediated degradation of SATB1. *J Cell Commun Signal*. 2023;17(3):993–1008. <https://doi.org/10.1007/s12079-023-00751-0>.
 29. Zhou J, Zhao Y, An P, Zhao H, Li X, Xiong Y. Hsa_circ_0002348 regulates trophoblast proliferation and apoptosis through miR-126–3p/BAK1 axis in preeclampsia. *J Transl Med*. 2023;21(1):509. <https://doi.org/10.1186/s12967-023-04240-1>.
 30. Lv Z, Lv DY, Meng JY, et al. Trophoblastic mitochondrial DNA induces endothelial dysfunction and NLRP3 inflammasome activation: implications for preeclampsia. *Int Immunopharmacol*. 2023;114:109523. <https://doi.org/10.1016/j.intimp.2022.109523>.
 31. Hong M, Tao S, Zhang L, et al. RNA sequencing: new technologies and applications in cancer research. *J Hematol Oncol*. 2020;13(1):166. <https://doi.org/10.1186/s13045-020-01005-x>.
 32. Wang Y, Yuan Y, Wang W, et al. Mechanisms underlying the therapeutic effects of Qingfei Yin in treating acute lung injury based on GEO datasets, network pharmacology and molecular docking. *Comput Biol Med*. 2022;145:105454. <https://doi.org/10.1016/j.combiomed.2022.105454>.
 33. Xie ZS, Zhao JP, Wu LM, et al. Hederagenin improves Alzheimer's disease through PPAR α /TFEB-mediated autophagy. *Phytomedicine*. 2023;112:154711. <https://doi.org/10.1016/j.phymed.2023.154711>.
 34. Wang Y, Jie L, Gong H, et al. miR-30 inhibits proliferation of trophoblasts in preeclampsia rats partially related to MAPK/ERK pathway. *Exp Ther Med*. 2020;20(2):1379–84. <https://doi.org/10.3892/etm.2020.8866>.
 35. Chen M, Chao B, Xu J, et al. CPT1A modulates PI3K/Akt/mTOR pathway to promote preeclampsia. *Placenta*. 2023;133:23–31. <https://doi.org/10.1016/j.placenta.2023.01.007>.
 36. Xu LZ, Li BQ, Li FY, et al. Upregulation of Wnt2b exerts neuroprotective effect by alleviating mitochondrial dysfunction in Alzheimer's disease. *CNS Neurosci Ther*. 2023;29(7):1805–16. <https://doi.org/10.1111/cns.14139>.
 37. Chen Q, Jiang S, Liu H, et al. Association of lncRNA SH3PXD2A-AS1 with preeclampsia and its function in invasion and migration of placental trophoblast cells. *Cell Death Dis*. 2020;11(7):583. <https://doi.org/10.1038/s41419-020-02796-0>.
 38. Tong D, Zhao Y, Tang Y, Ma J, Wang Z, Li C. Circ-Usp10 promotes microglial activation and induces neuronal death by targeting miRNA-152-5p/CD84. *Bioengineered*. 2021;12(2):10812–22. <https://doi.org/10.1080/21655979.2021.2004362>.
 39. Chen J, Chen T, Zhu Y, et al. circPTN sponges miR-145–5p/miR-330–5p to promote proliferation and stemness in glioma. *J Exp Clin Cancer Res*. 2019;38(1):398. <https://doi.org/10.1186/s13046-019-1376-8>.
 40. Cong P, Wu T, Huang X, et al. Identification of the Role and clinical prognostic value of target genes of m6A RNA Methylation regulators in glioma. *Front Cell Dev Biol*. 2021;9:709022. <https://doi.org/10.3389/fcell.2021.709022>.
 41. Morris R, Loftus A, Friedmann Y, Parker P, Pallister I. Intra-pelvic pressure changes after pelvic fracture: a cadaveric study quantifying the effect of a pelvic binder and limb bandaging over a bolster. *Injury*. 2017;48(4):833–40. <https://doi.org/10.1016/j.injury.2017.01.046>.
 42. Park M, Choi S, Kim S, et al. NF- κ B-responsive miR-155 induces functional impairment of vascular smooth muscle cells by downregulating soluble guanylyl cyclase. *Exp Mol Med*. 2019;51(2):1–12. <https://doi.org/10.1038/s12276-019-0212-8>.
 43. Witvrouwen I, Mannaerts D, Ratajczak J, et al. MicroRNAs targeting VEGF are related to vascular dysfunction in preeclampsia. *Biosci Rep*. 2021;41(8):BSR20210874. <https://doi.org/10.1042/BSR20210874>.
 44. He L, Song Q, Hu J, Wu J. Expression of HMGB1-TLR4 in placentas from preeclamptic pregnancies and its effect on proliferation and invasion of HTR-8/SVneo cells. *Gynecol Obstet Invest*. 2023;88(3):159–67. <https://doi.org/10.1159/000530006>.
 45. Ozmen A, Nwabuobi C, Tang Z, et al. Leptin-mediated induction of IL-6 expression in hofbauer cells contributes to preeclampsia pathogenesis. *Int J Mol Sci*. 2023;25(1):135. <https://doi.org/10.3390/ijms25010135>.

Publisher's Note

Springer Nature remains neutral with regard to jurisdictional claims in published maps and institutional affiliations.